Available online at www.sciencedirect.com
SCIENCE DIRECT®
ELSEVIER
Palaeogeography, Palaeoclimatology, Palaeoecology 236 (2006) 56–73
PALAEO
www.elsevier.com/locate/palaeo

Millennial-scale changes in terrestrial sediment input and Holocene surface hydrography in the northern South China Sea (IMAGES MD972146)

Da-Cheng Lin [a], Chiung-Hui Liu [a], Tien-Hsi Fang [b], Cheng-Han Tsai [b], Masafumi Murayama [c], Min-Te Chen [a,*]

[a] *Institute of Applied Geosciences, National Taiwan Ocean University, Keelung 20224, Taiwan, ROC*
[b] *Department of Marine Environmental Informatics, National Taiwan Ocean University, Keelung 20224, Taiwan, ROC*
[c] *Center for Advanced Marine Core Research, Kochi University, Kochi, Japan*

Received 30 September 2004; accepted 11 November 2005

Abstract

This study presents a high-resolution, multi-proxy analysis of sediments from IMAGES core MD972146 in the northern South China Sea (SCS). Analyses include detailed measurements of planktonic foraminifer oxygen isotopes, sediment carbonate, total organic carbon (TOC), opal, and phosphorus concentrations, as well as a Holocene interval of planktonic foraminifer sea surface temperature (SST) estimates. The age model of MD972146 was constructed by adopting oxygen isotope stratigraphy and AMS ^{14}C dating, and fine-tuned further by correlation with nearby, well-studied SONNE 17940 and Hulu stalagmite isotope records. The age model indicates that this record covers the past 70,000 yr—from isotope stage 4 to the Holocene—with a nearly constant, very high sedimentation rate of ~50 cm/kyr. Such sedimentation rates allow for intensive investigations of millennial-scale climate variability expressed in the SCS and its potential global linkages. We constructed a composite terrestrial index (CTI) for MD972146 through a principal component analysis of a suite of the core proxies that are sensitive to terrestrial sediment input. During the last glacial of stage 4 to stage 2, warm interstadials appear to coincide with high terrestrial sediment pulses inferred from the CTI, suggesting humid conditions in the SCS and Southern China. Intervals of high terrestrial input are also correlated with Heinrich events, suggesting an increase of eolian and possibly also of fluvial terrestrial input to the northern SCS. Our high resolution Holocene SST and salinity estimates show warm, stable and humid conditions during short episodes of quasi-periodic, millennial-scale cooling in the North Atlantic, superimposed on generally more humid conditions during the middle Holocene (4–6 ka) compared to the dry late Holocene (0–4 ka). The presented data provide evidence that a variety of mechanisms involving the strength of East Asian summer monsoons, migration of the Intertropical Convergence Zone, and processes that are analogous to those governing the El Niño Southern Oscillation and the Arctic Oscillation might play important roles in modulating tropical climate during the last glacial stages and the Holocene.

Keywords: Terrestrial sediment; Sea surface temperature; South China Sea; Glacial cycles; Holocene; Planktic foraminifer; Intertropical Convergence Zone

* Corresponding author.
E-mail address: mtchen@mail.ntou.edu.tw (M.-T. Chen).

0031-0182/$ - see front matter © 2006 Elsevier B.V. All rights reserved.
doi:10.1016/j.palaeo.2005.11.039

1. Introduction

Two conspicuous millennial-scale climate changes have been discovered in the last glacial period: Dansgaard–Oeschger events and Heinrich events (Heinrich, 1988; Dansgaard et al., 1993; Grootes et al., 1993). The Dansgaard–Oeschger events involved warm air temperature excursions over Greenland, with temperature oscillations of ~5–10 °C. The Heinrich events occurred when icebergs collapsed from the Laurentide Ice Sheet that covered North America to the North Atlantic Ocean, delivering a large quantity of ice-rafted debris (IRD) to the sea floor (Heinrich, 1988). Episodically high abundances of cold water species of planktic foraminifer *N. pachyderma* (left coiling) in deep-sea sediment cores from the North Atlantic Ocean were used to indicate the rapid cooling during the Heinrich events, and the more rapid warming following the events (Bond et al., 1992, 1993; Bond and Lotti, 1995). The millennial-scale changes were also documented in studies of Holocene North Atlantic sediment cores (Bond et al., 1997, 2001). Possible mechanisms responsible for the remarkable millennial-scale climate variability of the North Atlantic include changes in the formation rates of North Atlantic Deep Water, the flux of fresh water and transport of heat and moisture, and/or solar variability (Bond et al., 1997, 2001; Ganopolski and Rahmstorf, 2001; Bard, 2002; Claussen et al., 2003).

While modeling studies have failed to reproduce the full magnitude of the millennial-scale climate oscillations by prescribing only tropical climate perturbations (Ganopolski and Rahmstorf, 2001; Claussen et al., 2003), large synchronous variations of tropical–subtropical climate are suggested from paleoclimate studies on marine and terrestrial records (Porter and An, 1995; Chen et al., 1997; Schulz et al., 1998; Arz et al., 1998; Hendy and Kennett, 2000; Emmer and Thunell, 2000; Leuschner and Sirocko, 2000; Peterson et al., 2000; Wang et al., 2001; Suthhof et al., 2001; Hendy et al., 2002). Though the mechanisms that link low and high latitude climate variations on millennial time-scales are not fully understood, the disturbance of tropical hydrological cycles, and global climate oscillation patterns such as ENSO (El Niño Southern Oscillation), which closely involves equatorial sea surface temperature (SST), have the potential to reproduce short-term variations of wind fields and moisture transport and result in feedbacks that amplify the short-term variations (Bard, 2002; Stott et al., 2002; Koutavas et al., 2002; Claussen et al., 2003).

As the surface ocean of the western Pacific is a large source of moisture and heat that are important drivers in ENSO dynamics, and as the East Asian monsoon plays an important role in the latitudinal transport of moisture and heat, we aim in this study to assess the amplitude and phasing of climate change in a high-resolution sediment record from the South China Sea (SCS) in the western Pacific (IMAGES core MD972146, Fig. 1). The SCS is the largest marginal sea of the Western Pacific, and the East Asian monsoon dominates the climate of the SCS. The monsoon system is driven by the different thermal responses of the land and ocean to seasonal solar insolation. Seasonal changes in the monsoon winds have an important effect on the conditions of sea-surface circulation, hydrography, chemistry, biological production and sediment composition (Wyrki, 1961; Shaw and Chao, 1994; Shaw et al., 1996; Wiesner et al., 1996; Huang et al., 1997a,b; Wang et al., 1999a,b,c; Kuo et al., 2000; Liu et al., 2002; Gao and Zhou, 2002; Higginson et al., 2003; Tamburini et al., 2003). During the Northern Hemisphere summer (May to September), when the Intertropical Convergence Zone (ITCZ) moves northward, the southwesterly wind drives humid and warm surface water from the equatorial Indian Ocean into the SCS. During the Northern Hemisphere winter (September to April) when the ITCZ moves southward, the stronger northeasterly winds drive high-latitude cold surface water, and also trigger southward intrusions of the Chinese Coastal and Kuroshio Currents from the Taiwan and Luzon Straits that lead to a latitudinal gradient of SST (Wyrki, 1961; Shaw and Chao, 1994; Shaw et al., 1996; Higginson et al., 2003) (Fig. 1).

The sediment cores taken from the SCS are ideal for the purpose of conducting this high-resolution, millennial-scale study, as the SCS contains undisturbed hemipelagic sediments with ultrahigh sedimentation rates. Studies on a nearby core SONNE 17940 (Wang et al., 1999a,b,c) with well-established age controls for the past 40 kyr show that the sedimentation rates in this area vary from ~20–80 cm/kyr, which are appropriate for analyzing millennial-scale climate signals. The SCS sediments also contain large fluxes of terrestrial sediments transported via large rivers (Pearl and Red Rivers in the north, and Mekong River in the south); thus the SCS sediment cores are highly suitable for studying and reconstructing relationships between continental precipitation and ocean climate. The site of core MD972146 is located offshore of the mouth of the Pearl River (Fig. 1); thus the effects of large precipitation events and discharge of fluvial sediments from the Pearl River into the SCS should be recorded in the sediments of the site. Previous studies conducted by analyzing SCS sediment cores have already documented surface hydrography and productivity patterns

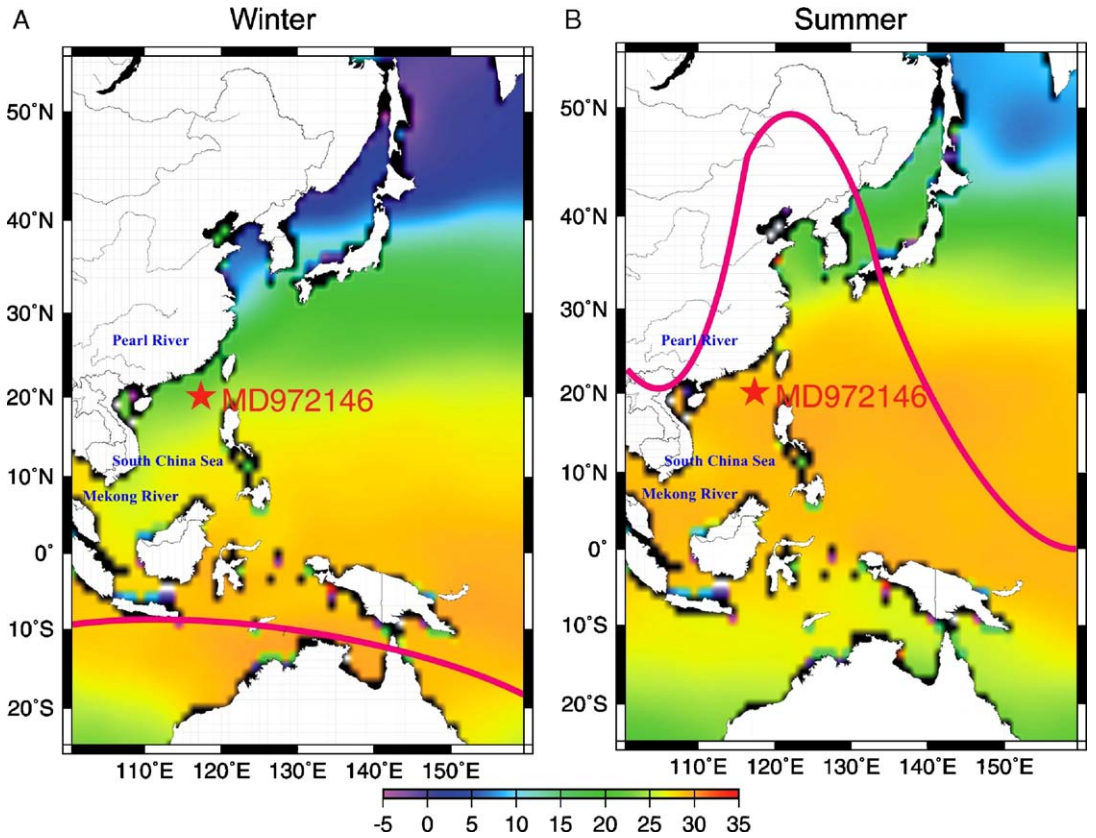

Fig. 1. Map of IMAGES MD972146 core location in the northern South China Sea (SCS). This site is near the mouth of the Pearl River which transports fluvial sediments to the SCS. Large continental shelves were exposed to the north during glacial sea level lowstands at the location of the Taiwan Strait where the present water depth is ~ 80–100 m. Seasonal distributions of sea surface temperature (SST) patterns and of the migration of the Intertropical Convergence Zone (ITCZ) are shown. (A) During winter (October to April), the ITCZ migrates to a southward position that is associated with stronger winter monsoons, which bring relatively cold and dry conditions to the northern SCS. (B) During Northern Hemisphere summer (May to September), the ITCZ moves to its most northward position with the development of stronger East Asian summer monsoons that bring warm and humid conditions to the northern SCS.

dominated by East Asian monsoons over past glacial–interglacial cycles (Wang et al., 1999a,b,c; Chen, 1999; Chen et al., 1999; Bühring et al., 2001; Higginson et al., 2003).

In this study, we attempted to use the newly available core MD972146 to study the millennial-scale variations of terrestrial input that reflect regional precipitation in Southern China and to reconstruct a high resolution SST record of the Holocene interval of the core. We used AMS ^{14}C dating as well as age correlations between the MD972146 planktic foraminifer *G. sacculifer* $\delta^{18}O$ and the $\delta^{18}O$ record of SONNE 17940 (Wang et al., 1999a,b,c) and Hulu Cave stalagmite records (Wang et al., 2001) for precise age control of the past 70 kyr of the core. Variations of carbonate, total organic carbon (TOC), detrital total inorganic phosphorus (detrital-TIP), TOC/TOP, and TOC/Total Nitrogen (TN) were measured to estimate past terrestrial input and precipitation. Planktic foraminifer faunal assemblages were counted for the Holocene interval of the core to estimate quantitative SSTs using the Modern Analogue Technique (MAT) (Prell, 1985) and Revised Analogue Method (RAM) (Waelbroeck et al., 1998), and to estimate sea surface salinity (SSS) by extracting the temperature influences from the planktic $\delta^{18}O$ of the core. We found that the last glacial stages are characterized by millennial-scale alternations in sediment terrestrial input in the SCS that indicate regional precipitation changes of the same scale. The Holocene SST and SSS records reconstructed from this core suggest warm, stable and humid conditions during short episodes of quasi-periodic, millennial-scale cooling in the North Atlantic. The SST and SSS records also show generally more humid conditions during the middle Holocene (4–6 ka) compared to the dry late Holocene (0–4 ka)

and suggest a characteristic tropical pattern during millennial-scale shifts of global climate.

2. Data and methods

2.1. IMAGES MD972146 core samples

We studied giant piston core MD972146 (20°07.019′ N, 117°23.08′E, water depth 1720 m, core length 38.69 m) collected from the northern slope of the SCS during an IMAGES 1997 *Marion Dufresne* cruise (Chen et al., 1998). The core sediments consist of dark gray nannofossil- and foraminifer-oozes with some radiolarians and diatoms and are generally undisturbed (Chen et al., 1998). We sampled the core every 4 cm (average sample resolution of ~80 years) and obtained a total of 904 samples for foraminifer stable isotope analyses, 971 samples for biogenic sediment content (C, N, P, opal, etc.) analyses, and 250 samples from the Holocene interval for census counting of planktic foraminifer faunal assemblages.

2.2. Foraminifer stable isotope and terrestrial sediment content

Specimens of the planktic foraminifer *G. sacculifer* of a 250–300 μm size range were used for the stable isotope analyses in the Leibniz-Laboratory for Radiometric Dating and Stable Isotope Research, Kiel University, Germany. The standard deviation of repeated measurements of foraminifer shell samples from several core depth intervals was less than ±0.1‰. Duplicate measurements were averaged.

In measuring terrestrial sediment components, wet sediment samples were dried in an oven at ~50 °C. The dry samples were then ground to fine powders and separated into several sub-samples. The total carbon (TC) and organic carbon (TOC) of the samples were determined by the combustion and fuming method with a HORIBA-EMIA-221V Carbon Analyzer (Chang et al., 1991). The carbonate content ($CaCO_3$) of the samples was calculated by total inorganic carbon (TIC), which was obtained from subtracting TOC from TC. The standard deviation of repeated measurements for the TC and TOC was ±0.01%.

The total nitrogen content (TN) of the samples was determined by a combustion method with the Perkin Elmer 2400 Series II CHNO/S Analyzer. Sub-samples of 1.5–2.5 mg were heated in an oven at 950 °C and transformed into N_2. TN contents of the samples were estimated by the partial pressure of N_2. The standard deviation of repeated measurements of TN is ±0.02%. The TOC/TN ratio of the samples was calculated for estimating terrestrial input in this study.

Phosphorus (P) contents of the sediment samples were determined using a four-step sequential extraction technique (Ruttenberg, 1992; Anderson and Delaney, 2000). We used a PERKIN ELMER Lambda Bio 20 spectrophotometer to calculate total (TP), inorganic (TIP), and organic P (TOP) contents. One solid phase of the inorganic phosphorus can be extracted for determining detrital total inorganic P (detrital-TIP). The detrital-TIP and TOC/TOP ratio were used here as proxies for terrestrial input in this study. The standard deviation of repeated measurements for the TP, TOP, and TIP was ±0.0003%.

2.3. Planktic foraminifer fauna SST estimates

In order to reconstruct high-resolution Holocene variations of SST and SSS in the northern SCS, we sampled from the top 10 m of core MD972146 for census counting of planktic foraminifer faunal assemblages. A total of 250 samples was taken at every 4 cm of the Holocene interval of the core and were subject to processing for the faunal analyses. All planktic foraminifer faunal census data presented in this study were generated on splits of the >150 μm size fraction containing at least 300 whole specimens. The taxonomy of planktic foraminifers used in this study follows the schemes in Parker (1962), Bé (1967) and Kipp (1976). The taxonomic scheme adopted here is consistent with that used in previous SCS paleoceanoraphic studies based on planktic foraminifer faunal records (Chen et al., 1998; Chen and Huang, 1998; Chen et al., 1999, 2003).

The foraminifer-based SST estimates for MD972146 have been made by applying a widely accepted method, the Modern Analogue Technique (MAT) (Prell, 1985), and also by a later one, the Revised Analogue Method (RAM) (Waelbroeck et al., 1998). In MAT, a squared chord distance is used to measure the dissimilarity between faunas of downcore and coretop samples, and selects a subset of most similar samples (analogues) from a coretop database as a basis for estimating the paleo-SSTs of the downcore samples. RAM SST estimates were performed for the first time on the western Pacific downcore data. The RAM was proposed to improve the estimation accuracy and precision of the MAT, adopting the same dissimilarity coefficient (i.e., squared chord distance) but with two important modifications: (1) reserving good analog coretop samples by examining the rate of a sharp increase in dissimilarity; and (2) remapping and interpolating the coretop fauna data base into a more homogenous, evenly

distributed space as a function of winter and summer SSTs. These modifications optimize the RAM applied to the coretop data from the western Pacific, where less-evenly distributed and/or less-well-preserved conditions might have limited the selection of good analogs for downcore estimates. The RAM calibration procedure provided an objective and dynamic threshold for excluding poor analogs, and searched for analogs based on a more expansive dataset. In this study, a threshold value of the dissimilarity increase rate of 0.6 was applied to reject poor analog coretop samples and, if there was no rejection, a maximum of the 10 best analogs were selected for calculating the non-weighted average of annual SSTs. The selection excluded the coretop samples from the same location as those samples have zero dissimilarities and provide redundant information.

The western Pacific coretop fauna data base (694 samples) was also expanded and added to with 466 data points by the RAM remapping procedure (with a grid step of 0.4 °C and an interpolation radius of 0.5 °C) in a winter and summer SST environmental space. In this study, we applied the MAT and RAM against a new western Pacific planktic foraminifer coretop database, which contains 694 samples compiled from the MARGO (Multiproxy Approach for the Reconstruction of the Glacial Ocean Surface) project (Chen et al., 2005). The difference in performance of the MAT and RAM for estimating SST has been demonstrated to be <1 °C with the use of the coretop database (Chen et al., 2005).

We calculated Holocene ΔSSS variations as the difference between the coretop and downcore values of MD972146. SSS was estimated by extracting the temperature effect on $\delta^{18}O$ from the corresponding planktic $\delta^{18}O$ values using the method of Martinez et al. (1997). We adopted a ratio of −0.23‰/°C (Duplessy et al., 1981) for calculating the temperature effect on the planktic $\delta^{18}O$, estimated SSS changes from the $\delta^{18}O$ residual by a ratio of +0.5‰/p.s.u. (Broecker, 1989), and assumed no significant sea level change in the SCS during the Holocene.

2.4. Age model

The *G. sacculifer* isotope record of MD972146 reveals shifts from the Holocene to the early stage 4 (Fig. 2). The $\delta^{18}O$ values vary from −2.3‰ to −0.3‰, with a maximum magnitude of glacial–interglacial oscillations of ~2.0‰, which is comparable with what has been reported from a nearby *G. ruber* record of SONNE 17940 (−3.0‰ to −1.0‰ over the past 40 kyr) (Wang et al., 1999a). As *G. ruber* is considered to be a shallower dwelling species than *G. sacculifer* (Hemleben et al., 1988), the 0.7‰ lighter offset in the *G. ruber* $\delta^{18}O$ record likely reflects the higher temperature or lower salinity in the shallow water where *G. ruber* lives. Despite the maximum lighter values in core 17940 observed at the beginning of stage 1 (Wang et al., 1999a), the MD972146 *G. sacculifer* $\delta^{18}O$ reaches maximum lighter values during middle stage 1 and maximum heavier values during stage 2 (Prell et al., 1986; Martinson et al., 1987), a glacial–interglacial pattern similar to the $\delta^{18}O$ record of SONNE 17940. Besides the major glacial–interglacial pattern, the $\delta^{18}O$ records of MD972146 and SONNE 17940 appear to share a similar structure of Bølling–Allerød (B/A) warming and Younger Dryas (YD) cooling since the initiation of deglaciation of the Last Glacial Maximum (LGM), as reported previously from Greenland ice core records (Alley et al., 1993; Stuiver et al., 1995). Short-lived, high frequency oscillations in the $\delta^{18}O$ in an amplitude of ~0.5–0.7‰ are also commonly observed in the Holocene and last glacial stages in both records.

Due to the overall similarity of the MD972146 and SONNE 17940 $\delta^{18}O$ records, we constructed a MD972146 age model for the past 40 kyr by correlation with SONNE 17940 (Fig. 2a). The age control points were selected from distinct changes in structure or large excursions common to both $\delta^{18}O$ records (Fig. 2a). This age model successfully converts the high resolution AMS ^{14}C chronology of SONNE 17940 and benefits further correlation of other proxies between the IMAGES and SONNE records.

We have also obtained seven AMS ^{14}C dates from MD972146 (mixed *G. ruber* and *G. sacculifer* specimens measured at Nagoya University, Japan). Each AMS ^{14}C age was corrected for a 400-year average reservoir age of Pacific surface water and was calibrated to calendar age by the CALIB 4.3 Program (Stuiver and Reimer, 1993) if the AMS ^{14}C age was younger than 20 ka, or by the formula of Bard et al. (1998) if older than 20 ka (Table 1).

For the MD972146 $\delta^{18}O$ record older than 40 ka, we also attempted to correlate our record with the $\delta^{18}O$ stalagmite record from Hulu Cave, Nanjing, southern China (Wang et al., 2001) (Fig. 2b). The Hulu Cave $\delta^{18}O$ record has been interpreted mainly to reflect changes in summer monsoon precipitation. This precipitation could also exert a major control on planktic foraminifer $\delta^{18}O$ changes in the northern SCS through fluvial water input from the Pearl River (Wang et al., 1999b). Our age model for MD972146 between 40–70 ka assumes that large oscillations of $\delta^{18}O$ shown in MD972146 and Hulu Cave stalagmites in this time

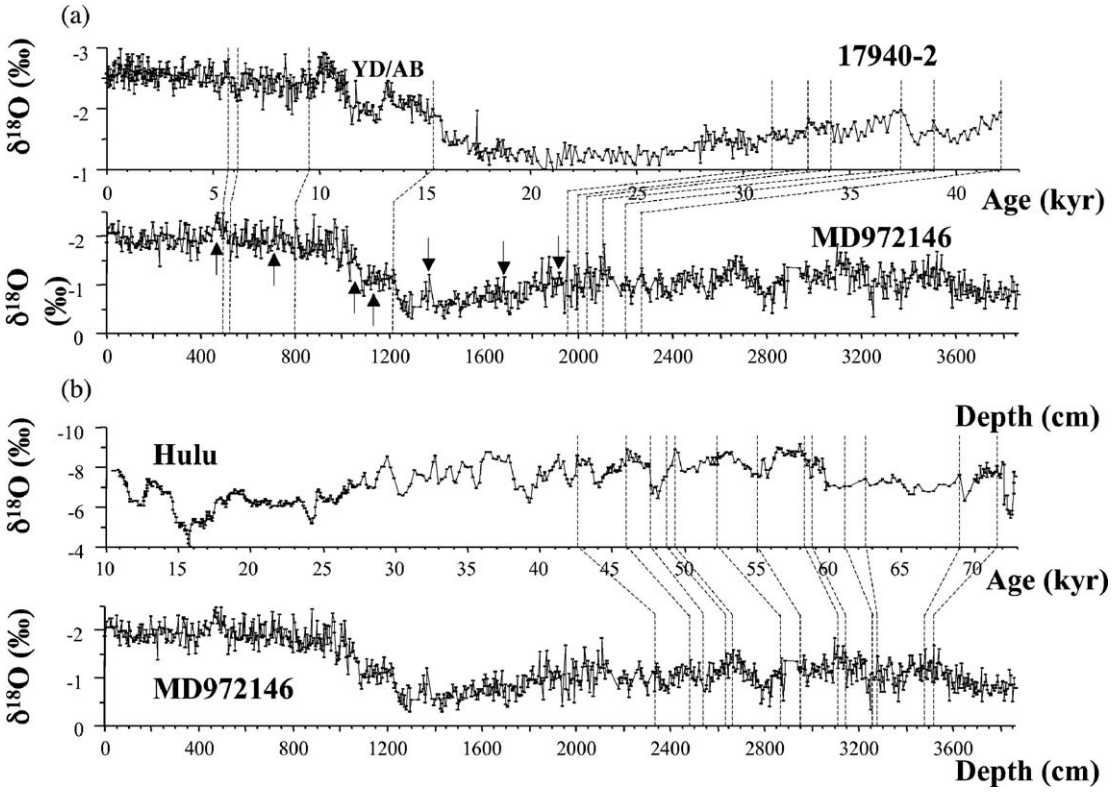

Fig. 2. Planktic foraminifer *G. sacculifer* δ^{18}O data measured from core MD972146 shown with the (a) correlation to the SONNE 17940 δ^{18}O record (Wang et al., 1999a) used to obtain age control points for the 0–40 ka interval of MD972146 [arrows indicate the MD972146 depth for AMS ^{14}C dating using planktic foraminifers (mixed samples of *G. ruber* and *G. sacculifer* specimens)] and (b) correlation with the Hulu Cave stalagmite δ^{18}O record (Wang et al., 2001) used to obtain age points for 40–70 ka of MD972146.

interval are driven by a common effect which translates East Asian summer monsoon precipitation signals rapidly into the terrestrial and marine records. This age tuning (Table 1) also transfers the high precision Hulu Cave ^{230}Th dating chronology (a version for H5 at 48 ka) into our MD972146 record and provides an independent view from marine oxygen isotopic age models. By a scatter plot of age versus depth of MD972146, our age model reveals an approximately stable sedimentation rate of ~50 cm/kyr (Fig. 3). A relatively high sedimentation rate of up to ~80–90 cm/kyr in the Holocene interval of MD972146 indicates sediment focusing on the upper slope of the basin during interglacials; such a high sedimentation rate is never found in the SCS. Our 4-cm sampling resolution results in a time resolution of 80 years on average and 40–50 years in the Holocene. Due to a lack of age control within stage 5.1 (5a) in MD972146, there might be large uncertainty in our age model for the bottom part of the record (60–70 ka). Our final age model was selected from many tests of different assignments of age control points for this interval and was chosen for use here as it constrained the sedimentation rate of the bottom part of the core in a reasonably constant range.

3. Results

3.1. Oxygen isotope and terrestrial input variations

The major features of the standard marine oxygen isotope record (Imbrie et al., 1984) are reproduced in our MD972146 planktic foraminifer *G. sacculifer* δ^{18}O measurements (Fig. 4). Our final age model establishes a record of ~70 kyr from oxygen isotope stage 4 to the Holocene. The δ^{18}O values vary between −2.3‰ and −0.3‰ and leave considerable room for interpreting the values as controlled by SST or SSS if we think the variation of global ice volume over this time interval only produces a maximum of ~1.0‰ changes in sea water composition of δ^{18}O (Schrag et al., 1996). The whole δ^{18}O record is marked by several distinct, short-term oscillations with average amplitudes of ~0.5–0.7‰. These oscillations are more pronounced in glacial stages 2–4.

Table 1
MD972146 age model

Age control depth (cm)	Calendar age (kyr)	C-14 age (kyr)	Sources
467.5	4.505	4.37±0.08	AMS ^{14}C
491.5	5.718	5.718	17940-2 (294.5 cm)
527.5	6.120	6.120	17940-2 (314.5 cm)
719.5	7.202	6.66±0.06	AMS ^{14}C
803.5	9.543	9.543	17940-2 (502.5 cm)
1051.5	10.974	10.09±0.04	AMS ^{14}C
1119.5	12.847	11.21±0.04	AMS ^{14}C
1215.5	15.374	15.374	17940-2 (798.5 cm)
1365.5	16.743	14.46±0.045	AMS ^{14}C
1683.5	27.166	23.49±0.08	AMS ^{14}C
1911.5	28.256	24.44±0.15	AMS ^{14}C
1955.5	31.329	31.329	17940-
1987.5	33.049	33.049	2 (1136.5 cm)
2039.5	34.144	34.144	17940-
2111.5	37.433	37.433	2 (1180.5 cm)
2203.5	39.000	39.000	17940-
2267.5	42.133	42.133	2 (1208.5 cm)
2339.5	42.964	42.964	17940-
2483.5	46.283	46.283	2 (1252.5 cm)
2547.5	47.920	47.920	17940-
2639.5	48.830	48.830	2 (1272.5 cm)
2667.5	49.450	49.450	17940-
2875.5	53.230	53.230	2 (1312.5 cm)
2955.5	55.479	55.479	Hulu Cave
3115.5	57.988	57.988	Hulu Cave
2147.5	58.777	58.777	Hulu Cave
3255.5	61.378	61.378	Hulu Cave
3271.5	62.441	62.441	Hulu Cave
3479.5	68.973	68.973	Hulu Cave
3515.5	71.939	71.939	Hulu Cave

Terrestrial input variations recorded at this site were estimated by subtracting out the biogenic sediment content of carbonate (plotted as non-carbonate% [100 −carbonate%]), TOC, detrital-TIP, and ratios of TOC/TOP and TOC/TN (Fig. 4). It is worth noting that the variation patterns of these proxies for terrestrial input of the past 70 kyr share little similarity with those of glacial–interglacial cycles shown dominantly in the planktic foraminifer δ^{18}O record. Rather, these patterns appear to exhibit more short-term and high-frequency oscillations that are independent of the major glacial–interglacial stages. Many previous studies have suggested that terrestrial dilution in the SCS increased during major glacial stages, as large exposure of continental shelves may favor greater transport of terrestrial sediments into the deep sea (Wang et al., 1995). The MD972146 terrestrial proxies, however, show no such pattern of glacial increases and appear to be insensitive to sea level fluctuations of the past glacial–interglacial cycles.

Visual inspection of these five proxy records shows some similar time intervals of increased terrestrial input, indicating a common effect attributable to the terrestrial influence (Fig. 4). For example, in the broad time intervals of 14–18 ka (except for 100−carbonate%), 22–24, 38–43 (except for detrital TIP), 48–52, and 59–62 ka, these proxies suggest high terrestrial input. It appears that all five proxy records are linked to terrestrial input variations but are complicated by other processes particular to the individual proxy, such as differential preservation, biological productivity, and/or oceanographic processes. To evaluate a common effect that is more directly linked to terrestrial input, we assessed the variance in common among the five proxy records by extracting the first principal component from the records using a principal component analysis (PCA). We first interpolated each record to a common 300-year sample interval (the average time resolution of the records), and standardized each to unit variance. The first component, which we called a composite terrestrial index (CTI), indicates 37% of the total variance in the five records is explained by a common effect related to the variations of terrestrial input (Table 2). The high CTI values, as observed from a *R*-mode matrix of the PCA, are more positively correlated with TOC/TN, TOC, and TOC/TOP and are used to indicate high terrestrial input to core MD972146.

The pattern shown in the CTI variations of the past 70 kyr is similar to that of the five proxy records for terrestrial input, which is characterized not by major

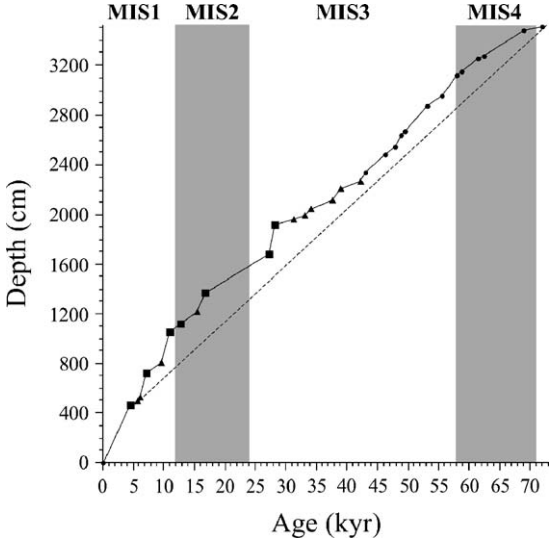

Fig. 3. Depth–age scatter plots for core MD972146 and age control points [squares: MD972146 AMS ^{14}C dating; triangles: tie points from correlation of the SONNE 17940 record (Fig. 2a); dots: tie points from the correlation of the Hulu Cave stalagmite record (Fig. 2b)]. Average sedimentation rate calculated on the basis of the age model is ~50 cm/kyr while the Holocene sedimentation rate is ~80–90 cm/kyr.

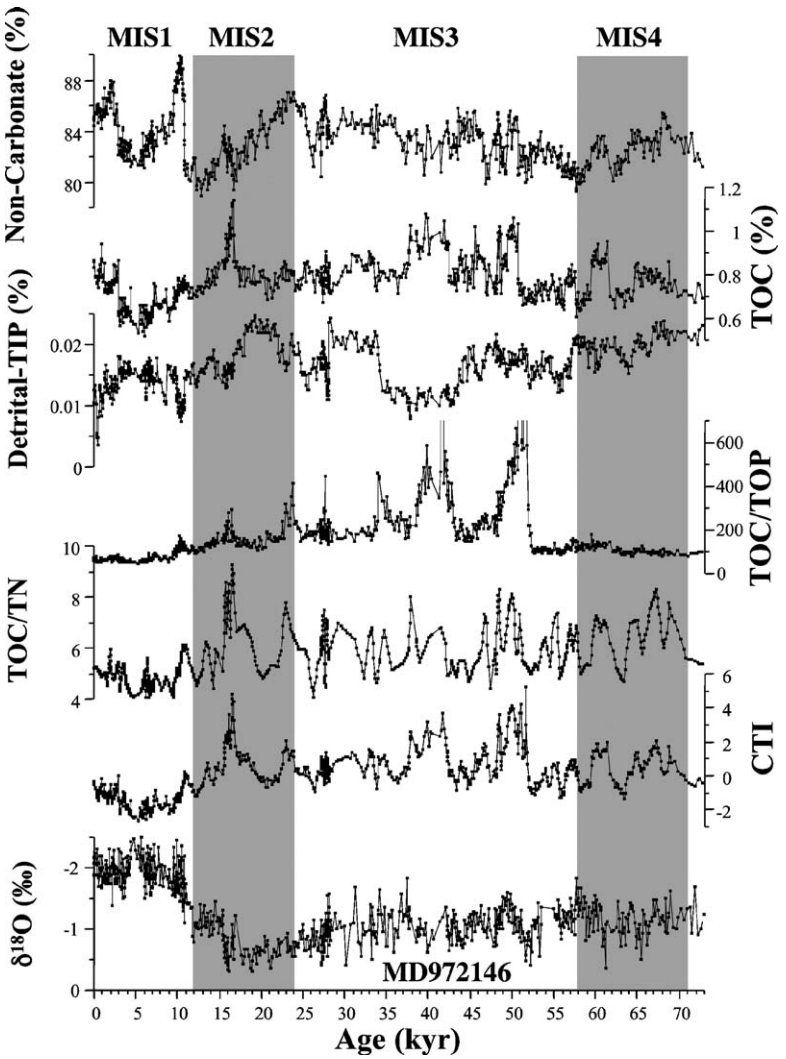

Fig. 4. MD972146 terrestrial sediment proxies of carbonate (plotted as non-carbonate%, i.e., [100S − carbonate%]), total organic carbon (TOC), detrital total inorganic phosphorus (detrital-TIP) contents, and ratios of TOC/total organic phosphorus (TOP), TOC/total nitrogen (TN) variations plotted versus age. A CTI (Composite Terrestrial Index) was calculated from a principal component analysis (PCA) of the five proxies of terrestrial sediment input in MD972146. The CTI was the first principal component and explains 37% of the variance of the five proxies. The *R*-mode PCA matrix is shown in Table 2.

glacial–interglacial change but by short-term oscillations (Fig. 4). The CTI values are high in the time intervals centered at 16–17, 23–24, 40–41, 49–50, and 60–61 ka (Fig. 4). During the middle Holocene, the CTI and the other four proxy records (non-carbonate%, TOC, TOC/TN, TOC/TOP) all consistently show low values, indicating low terrestrial input (Fig. 4).

3.2. Holocene planktic foraminifer SST and SSS variations

We have produced a high-resolution Holocene MD972146 record of planktic foraminifer faunal assemblages and SST and SSS estimates. A total of 23 planktic foraminifer species were thus identified in this study and the relative abundance of each species is expressed as a percentage of the total faunal assemblage. Our faunal analysis shows that the foraminifer assemblages in MD972146 are dominated by seven species that constitute over 85% of the total fauna composition. In order of decreasing mean abundances, these seven species and their average abundances in core MD972146 are: *Globigerinita glutinata* (19.6%), *Globigerinoides ruber* (14.8%), *Globigerina bulloides* (12.9%), *Neogloboquadrina dutertrei* + *Globquadrina pachyderma* (right coiling) (9.8%), *Pulleniatina*

Table 2
R-model principal component analysis for composite terrestrial index (CTI)

Terrestrial sediment indices	PC 1 (CTI)	PC 2	PC 3	PC 4	PC 5
TOC	0.599	0.328	0.138	0.235	0.678
Detrital-$CaCO_3$	−0.108	0.648	0.369	−0.654	−0.066
Detrital-TIP	0.153	−0.679	0.292	−0.567	0.330
TOC/TN	0.620	−0.085	0.434	0.122	−0.637
TOC/TOP	0.472	0.065	−0.756	−0.425	−0.146
Variance	0.366	0.280	0.162	0.131	0.062

obliquiloculata (9.7%), *Globigerinoides sacculifer* (9.4%), and *Globigerina calida* (8.5%).

This tropical–subtropical faunal assemblage is typical of interglacial stages of the SCS (Chen and Huang, 1998; Chen et al., 1999). As the high-diversity downcore species variations reveal patterns that are complex and intercorrelated, we used a CABFAC Q-mode factor analysis (Klovan and Imbrie, 1971) to combine the species that covary and to identify statistically independent components.

Three factors that explain ~97% of the variance of the downcore faunal variations were identified (Fig. 5). The first factor (35% variance) is highly correlated with the abundances of *P. obliquiloculata*, *N. dutertrei* + *G. pachyderma* (right coiling), and *G. sacculifer*. The abundance of *P. obliquiloculata* has been found to be relatively high in the western equatorial Pacific (Chen and Prell, 1998) and this taxon has been considered as a Kuroshio indicator in Okinawa Trough sediment core studies (Ujiié and Ujiié, 1999; Jian et al., 2000a; Ujiié et al., 2003). The abundances of *N. dutertrei* are high along the western boundaries of the Pacific Ocean—particularly between Japan and Taiwan and in the SCS, Flores Sea, Banda Sea, and Coral Sea—and are believed to be associated with cold SST, upwelling, and high nutrient conditions (Chen and Prell, 1998). Both *P. obliquiloculata* and *N. dutertrei* are deep surface-water dwellers that are abundant at depths below the thermocline (Hemleben et al., 1988). High loadings of the first factor, which combines both species in the early Holocene interval of MD972146,

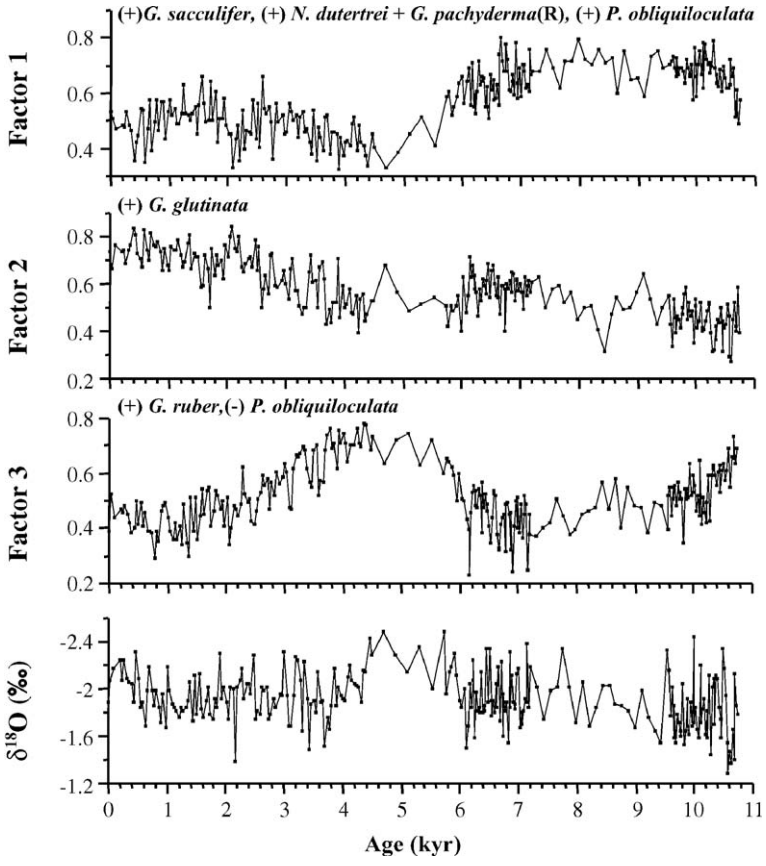

Fig. 5. MD972146 planktic foraminifer faunal factors analyzed from a *Q*-mode factor analysis using faunal abundance data from the Holocene (0–10 ka) interval of the core.

suggest a more oscillating climate mode that changes in the subsurface layer of the surface ocean in the SCS. The second factor is a monospecies *G. glutinata* factor (34% variance). *G. glutinata* have been found to be a part of western Pacific subtropical assemblages and more abundant at the edge areas of tropical assemblages (Chen and Prell, 1998). The long-term increase of this factor since the early Holocene as observed from the record (Fig. 5) might indicate a gradual cooling trend from the early to late Holocene in the northern SCS. The third factor (28%) shows a positive correlation with *G. ruber* abundances and negative correlation with *P. obliquiloculata*. As the abundances of *G. ruber* are generally high in the tropical western Pacific (Chen and Prell, 1998) with a more stratified, stable thermocline condition (Hemleben et al., 1988), we interpret the high loadings of factor 3 in the middle Holocene (4–6 ka) (Fig. 5) to

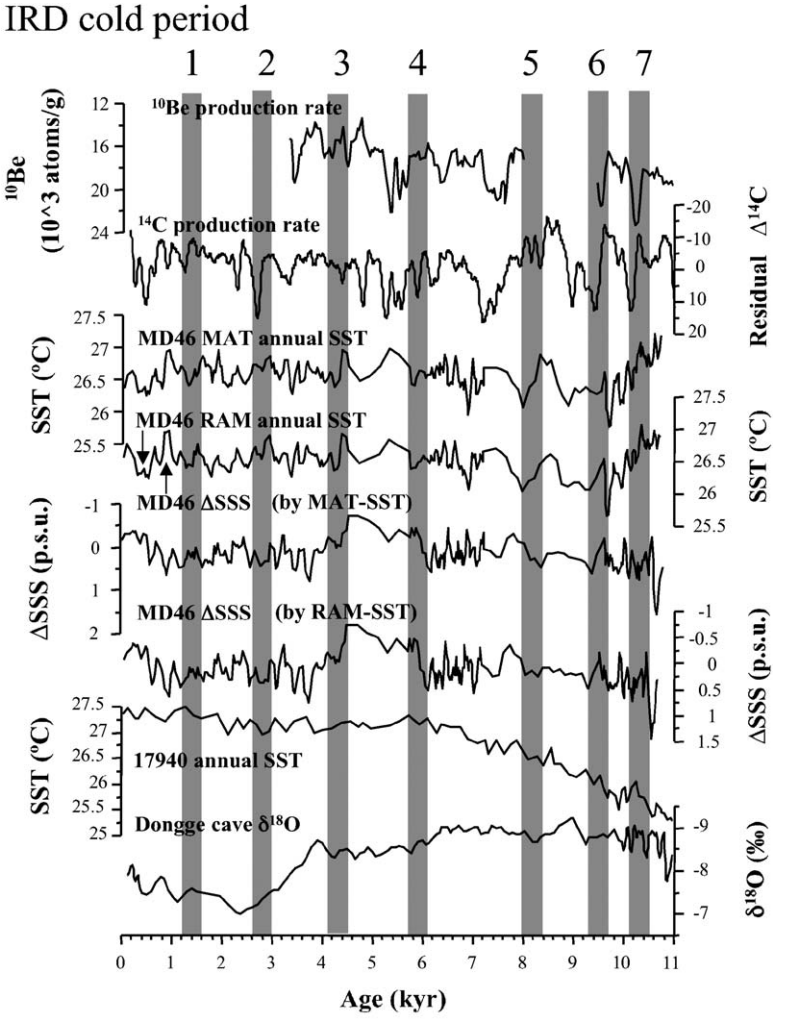

Fig. 6. MD972146 Holocene sea surface temperature (SST) and sea surface salinity (SSS) estimates compared with variations of cosmogenic ^{10}Be flux recorded in the GISP 2 ice core (Bond et al., 2001), and of excess ^{14}C (Δ^{14}C) recorded in tree rings (Stuiver et al., 1998). The short-term increase (shaded) of the ^{10}Be and Δ^{14}C are indicative of intervals with decreased solar activity that are linked to North Atlantic IRD cold events (Bond et al., 2001). The MD972146 SSTs were estimated by the MAT (Modern Analogue Technique) (Prell, 1985) and RAM (Revised Analog Method) (Waelbroeck et al., 1998) based on a new western Pacific coretop calibration (Chen et al., 2005). ?SSS estimates were calculated as the salinity (p.s.u.) differences between coretop and downcore samples from the planktic foraminifer δ^{18}O and MAT and RAM SSTs of MD972146 (Martinez et al., 1997). The SST and SSS variations indicate that the northern SCS Holocene climate was warm, stable and humid during the short episodes of North Atlantic cooling. The SST and SSS records clearly show relatively warm and humid conditions in the middle Holocene (4–6 ka) and cold and dry conditions in the late Holocene (0–4 ka). Arrows on the SST mark the timing of the Little Ice Age and Medieval Warm Period. The SONNE 17940 alkenone SST (Wang et al., 1999c) and the Dongge Cave δ^{18}O records (Yuan et al., 2004) are shown at the bottom for comparison.

indicate relatively warm temperatures with less disturbance in the surface water column in the northern SCS.

MAT and RAM SST estimates from core MD972146 exhibit a consistent pattern, with a range of maximum to minimum SSTs of ~1.2 °C in the Holocene (Fig. 6). This indicates relatively stable condition compared to what has been found in glacial, northern high-latitude records in the same interval (Bond et al., 1997, 2001). Within the apparently stable SST pattern, our MD972146 records also reveal ~0.3–0.8 °C short term oscillations, though these are within the general 1 °C uncertainty of the SST estimation techniques applied in a western Pacific coretop data set (Chen et al., 2005). We feel that fauna-based SST estimation for SCS records may have a much smaller uncertainty compared to other parts of the western Pacific, as the coretop database of the SCS used for calibrating SST is of high quality and has good distribution. Our MAT and RAM SST estimates also show very good analogues (a squared chord distance < 0.2) for the MD972146 down-core samples, so the uncertainty range commonly shown in MAT and RAM should be significantly reduced. Despite the uncertainty of the MAT and RAM, we observed a SST maximum in the middle Holocene of 4–6 ka. The SST records of the early and late Holocene appear to show equally cool conditions relative to the middle Holocene. The early Holocene (6–10 ka) interval is characterized by much larger SST oscillations of ~0.5–0.8 °C, while the late Holocene (0–4 ka) oscillations are smaller (0.3–0.5 °C).

The ΔSSS estimates made by extracting the MAT and RAM SST component of $\Delta\delta^{18}O$ from the $\delta^{18}O$ also show an approximately consistent pattern, with variations of ~1.5 p.s.u. in the Holocene (Fig. 6). The ΔSSS values in the middle Holocene interval (4–6 ka) appear to indicate fresher conditions, with decreases of SSS of ~0.5 p.s.u. The ΔSSS values of the early (6–10 ka) and late Holocene (0–4 ka) intervals show saltier conditions that are characterized by larger oscillations of ~0.5–0.6 p.s.u. (on average).

4. Discussion

4.1. Millennial-scale terrestrial input and precipitation

The coring site of MD972146 in the northern SCS is located near the mouth of the Pearl River (Fig. 1), where large quantities of fluvial sediments are transported from the drainage basins of the river in southern China. Increased humidity and higher precipitation rates in the Pearl River drainage basin would increase erosion and river runoff, and thus increase the supply of fluvial sediments to the upper slope of the northern SCS. During the last glacial stages, when global sea level fell by ~100 m, the large exposure of continental shelves in the Taiwan Strait might have provided another important source of fluvial sediments transported to the northern SCS. Recent seismic surveys of the submarine topography of the areas off southwestern Taiwan (Yu and Chuang, 2002) indicate the existence of large submarine canyons that represent significant down-cut channels of large paleo-rivers which might have transported sediments from inland southwestern Taiwan to the northern SCS during glacial stages. Eolian sediments (loess), carried mainly by East Asian winter monsoons, should also be a major contributor to the terrestrial sediments deposited in the northern SCS. Though distinguishing fluvial from eolian sediments in deep-sea cores is generally difficult, previous studies have proposed that abundances of silt modal grain size (>6 μm) (Wang et al., 1999a) and of pollen grains from semiarid and Alpine regions (Sun and Li, 1999) indicate glacial increases of eolian input to the northern SCS. However, no significant increase of terrestrial dilution or decrease of carbonate content in glacial stages was observed in MD972146 (Fig. 4), a pattern inconsistent with the hypothesis of glacial increases of eolian input. As tropical cyclones (typhoons) prevail from June to September in the SCS and western Pacific (Matsuura et al., 2003), their strong winds and high precipitation could provide more energy for transporting large fluxes of either eolian or fluvial sediments with larger grain sizes into the SCS. Our CTI record of core MD972146 appears to occur irrespective of cold or warm events, indicating the complexity of different sources of terrestrial sediments to the SCS (such as fluvial or eolian) in the past glacial to interglacial.

Large-amplitude and short-term oscillations in the planktic foraminifer $\delta^{18}O$ and CTI records (Fig. 4) indicate rapid changes in surface hydrography and terrestrial input in the northern SCS. As we have tied our $\delta^{18}O$ record to SONNE 17940 (Wang et al., 1999a) and to the Hulu Cave stalagmite $\delta^{18}O$ (Wang et al., 2001) records in the development of MD972146 age models, our interpretation is internally consistent with those for these two published records. We separated our data presentations into three figures: the Holocene (Fig. 6), 10–25 ka (Fig. 7), and 25–70 ka (Fig. 8). Based on our observations, the short-term oscillations of the CTI appear to share a similar structure with those exhibited in GISP 2 $\delta^{18}O$ (Dansgaard et al., 1993; Grootes et al., 1993), Hulu Cave stalagmite $\delta^{18}O$ (Wang et al., 2001), and Cariaco Basin core ODP1002C Ti content and color

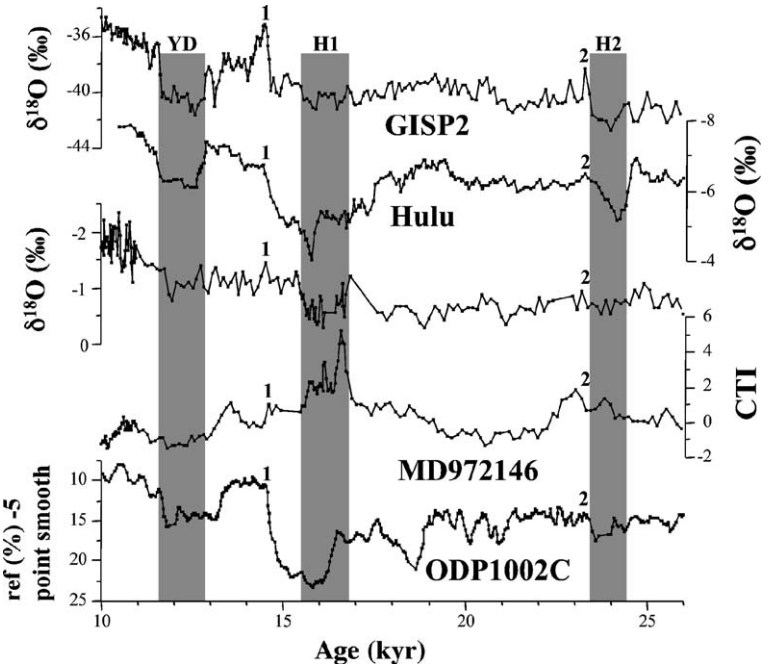

Fig. 7. A 10–25 ka interval of MD972146 composite terrestrial index (CTI) variations compared to GISP 2 ice core (Dansgaard et al., 1993; Grootes et al., 1993) and Hulu Cave stalagmite $\delta^{18}O$ (Wang et al., 2001), and to a tropical Atlantic ODP1002C record of color reflectance from the Cariaco Basin (Peterson et al., 2000). Cold intervals of the Heinrich events and Younger Dryas are shaded and the warm interstadial episodes are marked with numbers.

reflectance (Peterson et al., 2000). Within the uncertainty of our age controls, high CTI values of MD972146 appear to be associated with interstadials in GISP 2 $\delta^{18}O$ (Dansgaard et al., 1993; Grootes et al., 1993) and to be synchronous with increases in summer monsoon precipitation in southern China (Wang et al., 2001) and increases in precipitation, river runoff and terrestrial input to the Cariaco Basin (Peterson et al., 2000). Though the planktic $\delta^{18}O$ record of MD972146 shows more oscillations than the CTI record, lighter $\delta^{18}O$ values are accompanied by higher CTI in these interstadial events, suggesting that these short-term increases in terrestrial input are the result of increased fluvial input, which causes changes in SSS in the northern SCS. As short-term oscillations in Chinese loess records show a decrease of eolian transport in interstadials (Porter and An, 1995), the eolian input to the SCS was not likely to have increased in the interstadials. Lighter $\delta^{18}O$ of planktic foraminifer coincident with interstadials was also reported from SCS records with independent age control using high-resolution AMS ^{14}C dating (Wang et al., 1999a; Bühring et al., 2001), supporting our interpretation of SSS decreases during interstadials. A mechanism involving northward migration of the ITCZ was invoked to explain interstadial increases of fluvial input in the Cariaco Basin (Peterson et al., 2000), while peaked summer monsoon strength drives the ITCZ to its most northerly position in the SCS (Fig. 1). Larger amplitude oscillations of the MD972146 CTI, particularly visible in glacial stages (Fig. 4), might be the result of an expansion of shelves and the emergence of Taiwan Strait areas associated with sea level falls, which made the northern SCS more sensitive to fluvial input and regional precipitation. Though still preliminary, our data suggest a possible millennial-scale synchroneity of high fluvial terrestrial input and low SSS in the SCS, with a strong summer monsoon and northward migration of the ITCZ during events corresponding to interstadials. This also implies a connection with a La Niña-like condition in the western Pacific (Stott et al., 2002). In Stott et al.'s framework, the interstadial climate is analogous to the La Niña phases of modern ENSO, where the strongest vertical convection shifts longitudinally to Southeast Asia and brings large amounts of precipitation to the western tropical Pacific. With this connection, our SCS results imply a shift of such climatic features of more regional scale in the western tropical Pacific on millennial time scales.

The most prominent and episodically increased MD972146 CTI values during the time intervals corresponding to North Atlantic Heinrich cold events

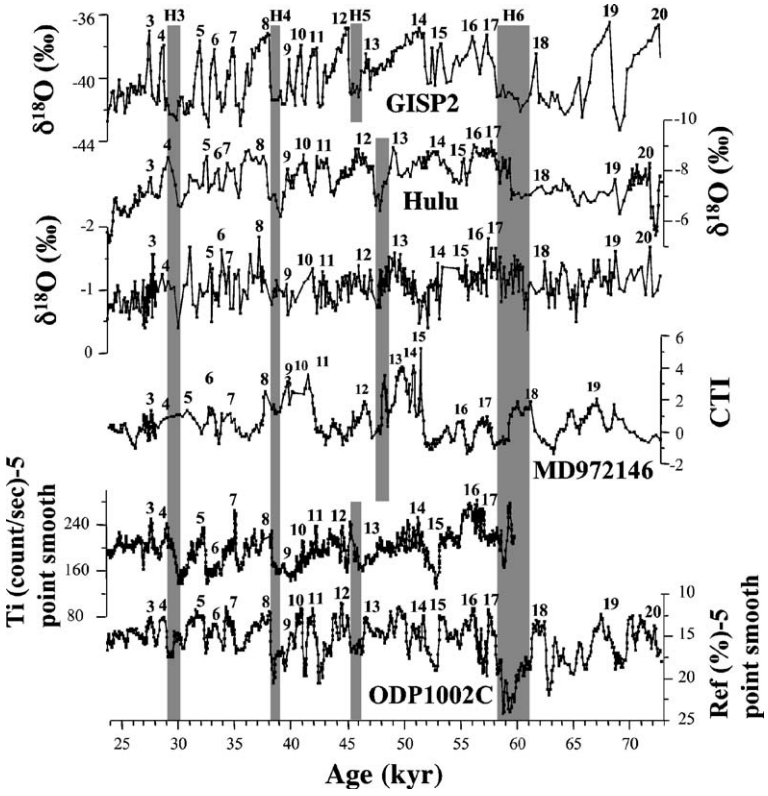

Fig. 8. A 25–70 ka interval of MD972146 composite terrestrial index (CTI) variations compared to GISP 2 ice core (Dansgaard et al., 1993; Grootes et al., 1993) and Hulu Cave stalagmite $\delta^{18}O$ (Wang et al., 2001), and to the tropical Atlantic ODP1002C records of Ti element content and color reflectance from Cariaco Basin (Peterson et al., 2000). Cold intervals of the Heinrich events and Younger Dryas are shaded and the warm interstadial episodes are marked with numbers.

(~16, 24, 30, 39, 46, 60 ka) (Bond et al., 1992, 1993; Bond and Lotti, 1995) might be the result of increases in both eolian and fluvial input to the SCS (Figs. 7 and 8). In Chinese loess eolian records (Porter and An, 1995), evidence already exists for increased eolian transport during Heinrich events. It has been suggested that strong winter monsoons driven by the large cooling of the Eurasian continent cause increased surface water mixing and high productivity in the SCS during Heinrich intervals (Chen et al., 1999; Higginson et al., 2003). In a study of SONNE 17940 records, Wang et al. (1999a) argued for an increase of eolian input during Heinrich event intervals, a finding primarily based on an empirical relationship between increased abundances of silt modal grain size (>6 μm) and eolian sediment sources. Quantifying the different contributions from eolian and fluvial sediment sources to MD972146 core was not an objective of this study but does merit future attention. However, we observed that the high CTI values during the intervals of Heinrich events correlate well with high TOC, TOC/TOP, and TOC/TN values (Fig. 4; Table 2). These correlations indicate enhanced terrestrial organic matter input, for which large fluvial transporting mechanisms might be responsible. Millennial-scale dry conditions, possibly indicating more frequent El Niño events during the cold Heinrich events, were suggested recently based on pollen and peat humification measurements from a record in northern Australia (Turney et al., 2004). These were explained by their coincidence with perihelion conditions in either the Northern Hemisphere spring or autumn in semi-precessional cycles. Longer-term, orbital scale El Niño-like conditions find favorable conditions for development during perihelion in Northern Hemisphere spring or autumn (Clement et al., 1999), the seasons that are most important to the development of the high rainfall brought by the Mei-Yu front or late-autumn typhoons in the northern SCS and Taiwan areas (Liang et al., 1995). Excessive rainfall occurs abnormally in southeastern Asia under conditions where cold, high-pressure air over the center of the Eurasian continent to the north meets warm and humid low-pressure air in the western tropical Pacific to the south (Kang et al., 2002; Matsuura et al., 2003). If these climate mechanisms

were similarly important in determining the magnitude and intensity of precipitation over the drainage areas of rivers that discharged fluvial sediments into the northern SCS during Heinrich events, a significant portion of the increased terrestrial input shown by high MD972146 CTI values in these events could be explained by fluvial contributions.

4.2. Holocene SST and SSS variations

High-resolution climate reconstructions for the Holocene have identified a series of distinct, millennial-scale IRD events in the North Atlantic which indicate episodic cooling at ~1.4, 2.8, 4.2, 5.9, 8.1, and 9.4 ka (Bond et al., 1997). These are coincident with an increased flux of ^{10}Be recorded in ice cores (Bond et al., 2001) and excess ^{14}C recorded in tree rings (Stuiver et al., 1998), both of which imply decreased solar activity during these cold events (Fig. 6). The evidence for the fingerprint of this episodic Holocene cooling in the tropical Indo-Pacific is controversial. Planktic foraminifer isotope and faunal assemblage records from the Kuroshio, Okinawa Trough areas (Jian et al., 2000a), along with an upwelling record based on *G. bulloides* abundance and hematite content records from the Arabian Sea (Gupta et al., 2003), suggest a weakening of Kuroshio current intensity and of Indian summer monsoon strength during the cold events. In contrast, the SSS record of SONNE 17940 (Wang et al., 1999c) and precipitation estimates from the stalagmite δ^{18}O record of Dongge Cave in Guizhou, China (Yuan et al., 2004) (Fig. 6) appear to show no such abrupt cooling in the Holocene.

If the Holocene climate in the northern SCS is tightly linked to that in the North Atlantic, we should expect to observe a series of either rapid cooling or decreased SSS events in the SCS record at MD972146 nearly coincident with these cold events, because the winter monsoon strength should have increased relative to the summer monsoon due to the large cooling in the Eurasian continent and the stable warmth over the western Pacific. In fact, we observe no such change (Fig. 6). Rather, the MD972146 SST and SSS records exhibit relatively stable patterns during the time intervals of North Atlantic cooling and imply warm, stable and humid conditions in the northern SCS with very little variation in monsoon strength. Despite the lack of evidence for correlative events, the MD972146 SST and SSS records instead exhibit low-frequency changes: warmer and more humid conditions in the middle Holocene (4–6 ka) and a cold, dry climate in the late Holocene (0–4 ka). The 4–6 ka interval of warm and humid climate in the northern SCS is apparently linked with the disappearance of the cold water species *G. truncatulinoides* in the SCS and Okinawa Trough between 4–8 ka (Jian et al., 2000b), and a 4–9 ka interval of gradual return of higher summer monsoon precipitation in the Dongge Cave δ^{18}O records (Yuan et al., 2004). This millennial-scale climate change was also coincident with a short episode of aridity in southern Chile of the southeastern Pacific (Lamy et al., 2001). The correlation of these events across the Pacific shows a picture of climate oscillation patterns analogous to the shift to more La Niña-like conditions in the middle Holocene.

Alternatively, the late Holocene cold and dry climate in the SCS is consistent with Kuroshio sediment records revealing a pronounced *P. obliquiloculata* abundance minimum. This minimum indicates cooling or less intrusion and/or intensity of the Kuroshio Current in the Okinawa Trough (Ujiié and Ujiié, 1999; Jian et al., 2000a; Ujiié et al., 2003), while the Dongge Cave δ^{18}O record (Yuan et al., 2004) and the pollen record from the central Himalaya of India (Phadtare, 2000) exhibit decreased summer monsoon precipitation. By comparing this general pattern of cool, dry climate in the western Pacific to more humid conditions in the southeastern Pacific (Lamy et al., 2001), as well as to the southward displacement of the ITCZ inferred from a tropical Atlantic record (Haug et al., 2001), a picture emerges for the late Holocene of an El Niño-analogous event, which deserves more investigation in future studies.

Though still preliminary, our data suggest that the SCS climate did not respond to the short episodes of North Atlantic cooling that appear to constitute a 1470-year cycle in the Holocene (Bond et al., 1997). The Holocene SCS climate reconstructed from MD972146 instead shows more coherent patterns of climate changes on longer time scales, i.e., middle and late Holocene intervals, suggesting that mechanisms other than those driving the 1470-year cycle are important. One possible mechanism having global teleconnections involves the phases of the Arctic Oscillation (AO) (Thompson and Wallace, 1998), which may be important in determining the relationship among Northern Hemisphere high-latitude air temperature, North Pole sea–ice cover, Aleutian low and Siberian high pressure air, and East Asian monsoons. For example, one recent study (Gong et al., 2001) showed that there is significant correlation between late spring AO and the East Asian summer monsoon on interannual time scales, with Arctic cooling linked subsequently to increased rainfall in later seasons in southern China. If

the teleconnections were dominated by Holocene millennial-scale variability, our MD972146 SST and SSS data could provide evidence for further understanding such linkages.

5. Conclusions

Variations in planktic foraminifer $\delta^{18}O$ and a composite terrestrial index (CTI) derived from a suite of terrestrial sediment proxies, as well as high-resolution Holocene SST and SSS reconstructions in sediment core MD972146 from the northern SCS, imply millennial-scale climate changes linking low and high latitudes. The variations of the CTI are interpreted to be largely affected by fluvial and eolian input, though these two terrestrial components are not quantitatively distinguishable in this sediment record. Short-term oscillations of increased MD972146 CTI possibly reflect increased fluvial input and appear to coincide with warm interstadials in Greenland ice cores, higher precipitation in Hulu Cave stalagmite records from southern China, and Cariaco Basin marine records from the tropical Atlantic. Increased CTI values are also observed during the time intervals of Heinrich events, suggesting increased terrestrial input from potentially both eolian and fluvial sources. Holocene climate in the northern SCS remained warm and humid during the short cooling episodes of IRD deposition in the North Atlantic, suggesting a stability of tropical climate on shorter time scales. The relatively warm/humid middle Holocene (4–6 ka) and cold/dry late Holocene (0–4 ka) exhibited in the MD972146 SST and SSS records are considered to be coherent with large-scale patterns predicted by an ENSO-based climate dynamics. Our results imply that a variety of mechanisms involving strong teleconnections between the East Asian monsoon, the ITCZ, ENSO, and possibly the AO affect the millennial-scale variability of tropical climate.

Acknowledgments

This study is a contribution to the Taiwan IMAGES integrated project, National Science Council (NSC), Taiwan. We are grateful for the facility support we received from the Core Repository and Laboratory, National Center for Ocean Research (NCOR), Taiwan. This research was supported by the National Science Council (NSC92-2611-M-019-016), Academia Sinica (Asian Paleoenvironmental Changes (APEC) Projects), and the National Taiwan Ocean University, Taiwan. We thank L. Peterson, B.K. Khim, and M. Zhao for their constructive reviews.

References

Alley, R.B., Meese, D.A., Shuman, C.A., Gow, A.J., Taylor, K.C., Groote, P.M., White, J.W.C., Ram, M., Waddington, E.D., Mayewski, P.A., Zielinski, G.A., 1993. Abrupt increase in Greenland snow accumulation at the end of the Younger Dryas event. Nature 362, 527–529.

Anderson, L.D., Delaney, M.L., 2000. Sequential extraction and analysis of phosphorus in marine sediments: streamlining of the SEDEX procedure. Limnology and Oceanography 45 (2), 509–515.

Arz, H.W., Pätzold, J., Wefer, G., 1998. Correlated millennial-scale changes in surface hydrography and terrigenous sediment yield inferred from last-glacial marine deposits off Northeastern Brazil. Quaternary Research 50, 157–166.

Bard, E., 2002. Climate shock: abrupt changes over millennial time scales. Physics Today 55 (12), 32–37.

Bard, E., Arnold, M., Hamelin, B., Laborde, N.T., Cabioch, G., 1998. Radiocarbon calibration by mean of mass spectrometric $^{230}TH/^{234}U$ and ^{14}C ages of corals: an updated database including samples from Barbados, Mururoa and Tahiti. Radiocarbon 40 (3), 1085–1092.

Bé, A.W.H., 1967. Foraminifera, families: globigerinide and globorotaliidae. In: Fraser, J.H. (Ed.), Fiches d'Identification du Zooplancton. Cons. Int. Explor. Mer, Charlottenlund, Sheet, vol. 118.

Bond, G., Lotti, R., 1995. Iceberg discharges into the North Atlantic on millenial time scales during the last glaciation. Science 267, 1005–1010.

Bond, G., Heinrich, H., Broecker, W., Labeyrie, L., McManus, J., Andrews, J., Huon, S., Jantschik, R., Clasen, S., Simet, C., Tedesco, K., Klas, M., Bonani, G., Ivy, S., 1992. Evidence for massive discharges of icebergs into the North Atlantic Ocean during the last glacial period. Nature 360, 245–249.

Bond, G., Broecker, W., Johnsen, S., McManus, J., Labeyrie, L., Jouzel, J., Bonani, G., 1993. Correlations between climate records from North Atlantic sediments and Greenland ice. Nature 365, 143–147.

Bond, G., Showers, W., Cheseby, M., Lotti, R., Almasi, P., deMenocal, P., Priore, P., Cullen, H., Hajdas, I., Bonani, G., 1997. A pervasive millennial-scale cycle in North Atlantic Holocene and glacial climates. Science 278, 1257–1266.

Bond, G., Kromer, B., Beer, J., Muscheler, R., Evans, M.N., Showers, W., Hoffmann, S., Lotti-Bond, R., Hajdas, I., Bonani, G., 2001. Persistent solar influence on North Atlantic climate during the Holocene. Science 294, 2130–2136.

Broecker, W.S., 1989. The salinity contrast between the Atlantic and Pacific Ocean during glacial time. Paleoceanography 4 (2), 207–212.

Bühring, C., Sarnthein, M., Erlenkeuser, H., 2001. Toward a high-resolution stable isotope stratigraphy of the last 1.1 million years: site 1144, South China Sea. Proceedings of the Ocean Drilling Program. Scientific Results, vol. 184, pp. 77–107.

Chang, S.Y., Kao, S.J., Liu, K.K., 1991. Analysis of organic and carbonate in sediment (in Chinese). Acta Oceangraphica Taiwanica 27, 140–150.

Chen, Y.-Y., 1999. A late Quaternary paleoclimatic record of biogenic sediments from the South China Sea(in Chinese). Master Degree Thesis, National Taiwan Ocean University.

Chen, M.-T., Huang, C.-Y., 1998. Ice-volume forcing of winter monsoon climate in the South China Sea. Paleoceanography 13 (6), 622–623.

Chen, M.-T., Prell, W.L., 1998. Faunal distribution patterns of planktonic foraminifers in surface sediments of the low-latitude Pacific. Palaeogeography, Palaeoclimatology, Palaeoecology 137, 55–77.

Chen, F.H., Bloemendal, J., Wang, J.M., Li, J.J., Oldfield, F., 1997. High-resolution multi-proxy climate records from Chinese loess: evidence for rapid climatic changes over the last 75 kyr. Palaeogeography, Palaeoclimatology, Palaeoecology 130, 323–335.

Chen, M.-T., Beaufort, L., the Shipboard Scientific Party of the IMAGES III/MD106-IPHIS Cruise (Leg II), 1998. Exploring Quaternary variability of the East Asian monsoon, Kuroshio Current, and the Western Pacific warm pool systems: high-resolution investigations of paleoceanography from the IMAGES III/MD106-IPHIS cruise. Terrestrial, Atmospheric and Oceanic Sciences 9, 129–142.

Chen, M.-T., Wang, C.-H., Huang, C.-Y., Wang, P., Wang, L., Sarnthein, M., 1999. A late Quaternary planktonic foraminifer faunal record of rapid climatic changes from the South China Sea. Marine Geology 156, 85–108.

Chen, M.-T., Shiau, L.-J., Yu, P.-S., Chiu, T.-C., Chen, Y.-G., Wei, K.-Y., 2003. 500,000-year records of carbonate, organic carbon, and foraminiferal sea-surface temperature from the southeastern South China Sea (near Palawan Island). Palaeogeography, Palaeoclimatology, Palaeoecology 197, 113–131.

Chen, M.-T., Huang, C.-C., Pflaumann, U., Waelbroeck, C., Kucera, M., 2005. Estimating glacial western Pacific sea-surface temperature: methodological overview and data compilation of surface sediment planktic foraminifer faunas. Quaternary Science Reviews 24, 1049–1062.

Claussen, M., Ganopolski, A., Brovkin, V., Gerstengarbe, F.-W., Werner, P., 2003. Simulated global-scale response of the climate system to Dansgaard/Oeschger and Heinrich events. Climate Dynamics 21, 361–370.

Clement, A.C., Seager, R., Cane, M.A., 1999. Orbital controls on the El Niño/Southern Oscillation and the tropical climate. Paleoceanography 14 (4), 441–456.

Dansgaard, W., Johnsen, S.J., Clausen, H.B., Dahl-Jensen, D., Gundestrup, N.S., Hammer, C.U., Hvidberg, C.S., Steffensen, J. P., Sveinbjornsdöttir, A.E., Jouzel, J., Bond, G., 1993. Evidence for general instability of past climate from a 250-kyr ice-core record. Nature 364, 218–220.

Duplessy, J.-C., Be, A.W.H., Blanc, P.L., 1981. Oxygen and carbon isotope composition and biogeographic distribution of planktonic foraminifera on the Indian Ocean. Palaeogeography, Palaeoclimatology, Palaeoecology 33, 9–46.

Emmer, E., Thunell, R.C., 2000. Nitrogen isotope variations in Santa Barbara Basin sediments: implications for dentrification in the eastern tropical North Pacific during the last 50,000 years. Paleoceanography 15 (4), 377–387.

Ganopolski, A., Rahmstorf, S., 2001. Rapid changes of glacial climate simulated in a coupled climate model. Nature 409, 153–158.

Gao, R., Zhou, F., 2002. Monsoonal characteristics revealed by intraseasonal variability of sea surface temperature (SST) in the South China Sea(SCS). Geophysical Research Letters 29 (8) (63 1-4).

Gong, D.-Y., Wang, S.-W., Zhu, J.-H., 2001. East Asian winter monsoon and Arctic Oscillation. Geophysical Research Letters 28, 2073–2076.

Grootes, P.M., Stulver, M., White, J.W.C., Johnsen, S., Jouzel, J., 1993. Comparison of oxygen isotope records from the GISP2 and GRIP Greenland ice cores. Nature 366, 552–554.

Gupta, A.K., Anderson, D.M., Overpeck, J.T., 2003. Abrupt changes in the Asian southwest monsoon during the Holocene and their links to the North Atlantic Ocean. Nature 421, 354–357.

Haug, G.H., Hughen, K.A., Sigman, D.M., Peterson, L.C., Röhl, U., 2001. Southward migration of the Intertropical Convergence Zone through the Holocene. Science 293, 1304–1308.

Heinrich, H., 1988. Origin and consequences of cyclic ice rafting in the northwest Atlantic Ocean during the past 130,000 years. Quaternary Research 29, 142–152.

Hemleben, C., Spindler, M., Anderson, O.R., 1988. Modern Planktonic Foraminifera. Springer, New York.

Hendy, I.L., Kennett, J.P., 2000. Dansgaard–Oeschger cycles and the California Current System: planktonic foraminiferal response to rapid climate change in Santa Barbara Basin, Ocean Drilling Program Hole 893A. Paleoceanography 15 (1), 30–42.

Hendy, I.L., Kennett, J.P., Roark, E.B., Ingram, B.L., 2002. Apparent synchroneity of submillennial scale climate events between Greenland and Santa Barbara Basin, California from 30–10 ka. Quaternary Science Reviews 21, 1167–1184.

Higginson, M.J., Maxwell, J.R., Altabet, M.A., 2003. Nitrogen isotope and chlorin paleoproductivity records from the Northern South China Sea: remote vs. local forcing of millennial- and orbital-scale variability. Marine Geology 201, 1–28.

Huang, C.Y., Liew, P.M., Zhao, M., Chang, T.C., Kuo, C.M., Chen, M. T., Wang, C.H., Zheng, L.F., 1997a. Deep sea and lake records of the Southeast Asian paleomonsoons for the last 25 kyrs. Earth and Planetary Science Letters 146, 59–72.

Huang, C.Y., Wu, S.F., Zhao, M., Chen, M.T., Wang, C.H., Tu, X., Yuan, P.B., 1997b. Surface ocean and monsoon climate variability in the South China Sea since last glaciation. Marine Micropaleontology 32, 71–94.

Imbrie, J., Hays, J.D., Martinson, D.G., McIntyre, A., Mix, A.C., Morley, J.J., Pisias, N.G., Prell, W.L., Shackleton, N.J., 1984. In: Berger, et al. (Ed.), Milankovitch and Climate: Part 1. D. Reidel Publishing Company, pp. 269–305.

Jian, Z., Wang, P., Saito, Y., Wang, J., Pflaumann, U., Oba, T., Cheng, X., 2000a. Holocene variability of the Kuroshio Current in the Okinawa Trough, northwestern Pacific Ocean. Earth and Planetary Science Letters 184, 305–319.

Jian, Z., Wang, P., Chen, M.-P., Li, B., Zhao, Q., Buhring, C., Laj, C., Lin, H.-L., Pflaumann, U., Bian, Y., Wang, R., Cheng, X., 2000b. Foraminiferal responses to major Pleistocene paleoceanographic changes in the southern South China Sea. Paleoceanography 15, 229–243.

Kang, I.-S., Jin, K., Wang, B., Lau, K.-M., Shukla, J., Krishnamurthy, V., Schubert, S.D., Wailser, D.E., Stern, W.F., Kitoh, A., Meehl, G. A., Kanamitsu, M., Galin, V.Y., Satyan, V., Park, C.-K., Liu, Y., 2002. Intercomparison of the climatological variations of Asian summer monsoon precipitation simulated by 10 GCMs. Climate Dynamics 19, 383–395.

Kipp, N.G., 1976. New transfer function for estimating past seasurface conditions from sea-bed distribution of planktonic foraminiferal assemblages in the North Atlantic. In: Cline, R.M., Hays, J.D. (Eds.), Investigation of Late Quaternary Paleoceanography and Paleoclimatology. Memoir of Geological Society of America, vol. 145, pp. 3–41.

Klovan, J.E., Imbrie, J., 1971. An algorithm and FORTRAN-IV program for large-scale Q-mode factor analysis and calculation of factor scores. Mathematical Geology 3, 61–76.

Koutavas, A., Lynch-Stieglitz, J., Marchitto Jr., T.M., Sachs, J.P., 2002. El Nino-like pattern in ice age tropical Pacific sea surface temperature. Science 297, 226–230.

Kuo, N.-J., Zheng, Q., Ho, C.-R., 2000. Satellite observation of upwelling along the western coast of the South China Sea. Remote Sensing of Environment 74, 463–470.

Lamy, F., Hebbeln, D., Röhl, U., Wefer, G., 2001. Holocene rainfall variability in southern Chile: a marine record of latitudinal shifts of the Southern Westerlies. Earth and Planetary Science Letters 185, 369–382.

Leuschner, D.C., Sirocko, F., 2000. The low-latitude monsoon climate during Dansgaard–Oeschger cycles and Heinrich events. Quaternary Science Reviews 19, 243–254.

Liang, X.-Z., Samel, A.N., Wang, W.-C., 1995. Observed and GCM simulated decadal variability of monsoon rainfall in east China. Climate Dynamics 11, 103–114.

Liu, K.-K., Chao, S.-Y., Shaw, P.-T., Gong, G.-C., Chen, C.-C., Tang, T.Y., 2002. Monsoon-forced chlorophyll distribution and primary production in the South China Sea: observations and a numerical study. Deep-Sea Research I 49, 1387–1412.

Martinez, J.I., de Deckker, P., Chivas, A.R., 1997. New estimates for salinity changes in the Western Pacific Warm Pool during the Last Glacial Maximum: oxygen-isotope evidence. Marine Micropaleontology 32, 311–340.

Martinson, D.G., Pisias, N.G., Hays, J.D., Imbrie, J., Moore Jr., Theodore C., Shackleton, N.J., 1987. Age dating and the orbital theory of the ice ages: development of a high-resolution 0 to 300,000-year chronostratigraphy. Quaternary Research 27, 1–29.

Matsuura, T., Yumoto, M., Iizuka, 2003. A mechanism of interdecadal variability of tropical cyclone activity over the western North Pacific. Climate Dynamics 21, 105–117.

Parker, F.L., 1962. Planktonic foraminiferal species in Pacific sediments. Marine Micropaleontology 8, 219–254.

Peterson, L.C., Haug, G.H., Hughen, K.A., Röhl, U., 2000. Rapid changes in the hydrologic cycle of the tropical Atlantic during the last glacial. Science 290, 1947–1951.

Phadtare, N.R., 2000. Sharp decrease in summer monsoon strength 4000–3500 cal yr B.P. in the central higher Himalaya of India based on pollen evidence from Alpine peat. Quaternary Research 53, 122–129.

Porter, S.C., An, Z., 1995. Correlation between climate events in the North Atlantic and China during the last glaciation. Nature 375, 305–308.

Prell, W.L., 1985. The stability of low-latitude sea-surface temperatures: an evaluation of the CLIMAP reconstruction with emphasis on the positive SST anomalies. Rep TRO, vol. 25, pp. 1–60.

Prell, W.L., Imbrie, J., Martinson, D.G., Morley, J.J., Pisias, N.G., Shackleton, N.J., Streeter, H.F., 1986. Graphic correlation of oxygen isotope stratigraphy application to the late Quaternary. Paleoceanography 1 (2), 137–162.

Ruttenberg, K.C., 1992. Development of a sequential extraction method for different forms of phosphorus marine sediments. Limnology and Oceanography 37 (7), 1460–1482.

Schrag, D.P., Hampt, G., Murray, D.W., 1996. Pore fluid constraints on the temperature and oxygen isotopic composition of the glacial ocean. Science 272, 1930–1932.

Schulz, H., von Rad, U., Erlenkeuser, H., 1998. Correlation between Arabian Sea and Greenland climate oscillations of the past 110,000 years. Nature 393, 54–57.

Shaw, P.-T., Chao, S.-Y., 1994. Surface circulation of the South China Sea. Deep-Sea Research I 41 (11/12), 1663–1683.

Shaw, P.-T., Chao, S.Y., Liu, K.K., Pai, S.-C., Liu, C.-T., 1996. Winter upwelling off Luzon in the northeastern South China Sea. Journal of Geophysical Research 10 (C7), 16435–16448.

Stott, L., Poulsen, C., Lund, S., Thunell, R., 2002. Super ENSO and global climate oscillations at millennial time scales. Science 297, 222–226.

Stuiver, M., Reimer, P.J., 1993. Extend ^{14}C data base and revised CALIB 3.0 ^{14}C age calibration program. Radiocarbon 35, 215–230.

Stuiver, M., Braziunas, T., Groote, P., 1995. The GISP2 $\delta^{18}O$ climate record of the past 16,500 years and the role of the sun, ocean, and volcanoes. Quaternary Research 44, 341–354.

Stuiver, M., Reimer, P.J., Bard, E., Beck, J.W., Burr, G.S., Hughen, K. A., Kromer, B., McCormac, G., Plicht, J.V.D., Spurk, M., 1998. Intcal98 radiocarbon age calibration, 24,000–0 cal BP. Radiocarbon 40, 1041–1083.

Sun, X., Li, X., 1999. Pollen records of the last 37 ka in deep-sea core 17940 from the northern slope of the South China Sea. Marine Geology 156, 227–244.

Suthhof, A., Ittekkot, V., Gaye-Haake, B., 2001. Millennial-scale oscillation of denitrification intensity in the Arabian Sea during the late Quaternary and its potential influence on atmospheric N_2O and global climate. Global Biogeochemical Cycles 15 (3), 637–649.

Tamburini, F., Adatte, T., Föllmi, K., Bernasconi, S.M., Steinmann, P., 2003. Investigating the history of East Asian monsoon and climate during the last glacial–interglacial period (0–140,000 years): mineralogy and geochemistry of ODP Sites 1143 and 1144, South China Sea. Marine Geology 201, 147–168.

Thompson, D.W.J., Wallace, J.M., 1998. The Arctic Oscillation signature in the wintertime geopotential height and temperature fields. Geophysical Research Letters 25, 1297–1300.

Turney, C.S.M., Kershaw, A.P., Clemens, S.C., Branch, N., Moss, P.T., Flfield, L.K., 2004. Millennial and orbital variations of El Niño/Southern Oscillation and high-latitude climate in the last glacial period. Nature 428, 306–310.

Ujiié, H., Ujiié, Y., 1999. Late Quaternary course changes of the Kuroshio Current in the Ryukyu Arc region, northwestern Pacific Ocean. Marine Micropaleontology 37, 23–40.

Ujiié, Y., Ujiié, H., Taira, A., Nakamura, T., Oguri, K., 2003. Spatial and temporal variability of surface water in the Kuroshio source region, Pacific Ocean, over the past 21,000 years: evidence from planktonic foraminifera. Marin Micropaleontology 49, 335–364.

Waelbroeck, C., Labeyrie, L., Duplessy, J.-C., Guiot, J., Labracherie, M., Leclaire, H., Duprat, J., 1998. Improving past sea surface temperature estimates based on planktonic fossil faunas. Paleoceanography 13 (3), 272–283.

Wang, P., Wang, L., Bian, Y., Jian, Z., 1995. Late Quaternary paleoceanography of the South China Sea: surface circulation and carbonate cycles. Marine Geology 127, 145–165.

Wang, L., Sarnthein, M., Erlenkeuser, H., Grimalt, J., Grootes, P., Heilig, S., Ivanova, E., Kienast, M., Pelejero, C., Pflaumann, U., 1999a. East Asian monsoon climate during the Late Pleistocene: high-resolution sediment records from the South China Sea. Marine Geology 156, 245–284.

Wang, L., Sarntheih, M., Grootes, P.M., Erlenkeuser, H., 1999b. Millennial recoccurrence of century-scale abrupt events of East Asian monsoon: a possible heat conveyor for the global deglaciation. Paleoceanography 14 (6), 725–731.

Wang, L., Sarnthein, M., Erlenkeuser, H., Grootes, P.M., Grimalt, J.O., Pelejero, C., Linck, G., 1999c. Holocene variations in Asian monsoon moisture : a bidecadal sediment record from the South China Sea. Geophysical Research Letters 26, 2889–2892.

Wang, Y.J., Cheng, H., Edwards, R.L., An, Z.S., Wu, J.Y., Shen, C.-C., Dorale, J.A., 2001. A high-resolution absolute-dated late

Pleistocene monsoon record from Hulu Cave, China. Science 294, 2345–2348.

Wiesner, M.G., Zheng, L., Wong, H.K., Wang, Y., Chen, W., 1996. Fluxes of particulate matter in the South China Sea. In: Ittekkot, V., et al. (Ed.), Particle Flux in the Ocean. John Wiley & Sons, Ltd., pp. 293–312.

Wyrki, K., 1961. Scientific results of maritime investigations of the South China Sea and the Gulf of Thailand 1959–1961. Physical Oceanography of the Southeast Asian Waters. Scripps Institution of Oceanography, La Jolla, California, Naga Report, vol. 2.

Yu, H.-S., Chuang, C.-Y., 2002. Morphology and canyon forming processes of upper reach of the Penghu submarine canyon off Southwestern Taiwan. Terrestrial, Atmospheric and Oceanic Sciences 13, 91–108.

Yuan, D., Cheng, H., Edwards, R.L., Dykoski, C.A., Kelly, M.J., Zhang, M., Qing, J., Lin, Y., Wang, Y., Wu, J., Dorale, J.A., An, Z., Cai, Y., 2004. Timing, duration, and transitions of the last interglacial Asian monsoon. Science 304, 575–578.